Gain Scheduling Output Feedback Control for Vehicle Path Tracking Considering Input Saturation

Chao Liu [1], **Weiqiang Zhao** [2,*] and **Jie Li** [2]

1   Chassis & ADAS Department, SAIC Motor Technical Center, Shanghai 201800, China; cl15@mails.jlu.edu.cn
2   State Key Laboratory of Automotive Simulation and Control, Jilin University, Changchun 130022, China; lj@jlu.edu.cn
*   Correspondence: zwq@jlu.edu.cn; Tel.: +86-431-8509-5090

Abstract: This paper presents a gain scheduling output feedback control method to reduce driver workload and improve driving performance by considering input saturation. The driver–vehicle system model is developed by considering tire cornering stiffness uncertainties and different driver parameter uncertainties. Meanwhile, the input saturation is also considered in the driver-vehicle system. A quadratic Lyapunov function is designed to solve the optimization problem with uncertainties and input saturation. The results, which are based on the MATLAB-CarSim co-simulation platform, indicate that the robust controller not only improves the convergence rate of the state but also reduces the steering workload of the driver.

Keywords: robust control; gain scheduling output feedback; input saturation; intelligent vehicle; path following

1. Introduction

With the development of science and technology, the application of advanced driver assistance systems (ADASs), which help drivers reduce their workload and improve safety, has become increasingly possible. The DARPA (Defense Advanced Research Projects Agency) challenge in the United States has promoted the application of intelligent vehicles in daily life and has attracted worldwide attention. In Europe, many research institutes and universities have initiated research on the real-world safety benefits of ADASs and active safety systems. ADASs have advantages including reducing a driver's workload, facilitating more relaxed mental and physical activities, and increasing the driving safety potential [1]. ADASs also have the potential to optimize safety and efficiency in road traffic. For example, ADASs can correct the vehicle's trajectory and provide correct guidance to the driver with the steering wheel by direct controller intervention [2]. Due to the unpredictability of the driving environment, the driver needs to be alert to the control system and environment to handle any automation errors. As it is impossible to completely predict the driving environment, human supervision is considered necessary, especially when automated errors have serious consequences [3]. Driver characteristics must be implemented by using a realistic driver model to design a human–machine driving assistance system.

Many scholars have studied the characteristics of drivers for driving assistance system. Ref. [4] discuss the general design of personalized ADAS and propose a general conceptual framework to personalization in ADAS. Ref. [5] aims to examine how do driver gender, age, and aggression affect the performances and driver acceptances of typical ADAS. Based on the current machine learning approaches, Ref. [6] provides a survey on driving style characterization and recognition revising a variety of algorithms. In [7], two kinds of learning-based car-following personalized driver models were developed using naturalistic driving data. Ref. [8] identified teen drivers' perceived need for

ADASs, receptiveness to in-vehicle technology, and intervention preferences. A large number of driver assistance systems have been described in the scientific literature. Ref. [9] aimed to investigate consensus regarding the design, evaluation methods, and effectiveness of these systems. Ref. [10] presented a combined lateral and longitudinal driver model developed based on human subject driving simulator experiments that is able to identify different driver behaviors through driver model parameter identification. In [11], a lateral control method that redistributes the control effort between the steering angle and the brake is proposed. Meanwhile, the technique could facilitate the interaction between the driver and the assistance system while avoiding vehicle state saturation, including the tire force and steering angle. In [12], a driver-assistant control system with braking and steering functions is proposed to track the reference trajectory to ensure vehicle stability. In [13], an effective method to estimate the driving characteristic parameters of the general driver model is presented. To help the driver deal with handover scenarios smoothly, in [14], a robust controller is proposed to help the driver achieve better driving performance by considering different driver driving performances. To assist young drivers in tacking a given trajectory, in [15], a gain-scheduling controller is discussed, which considers driver parameters. In [16], the lateral shared control method is presented to ensure an excellent transfer of the control authority without generating harmful interference by considering the interaction between the controller and drivers. In [17], a human-centered steering assistant controller is proposed to realize sharing authority between the driver and the automatic copilot. By using a Gaussian distribution function with lateral deviation, the driving style, authority shifting, and authority conflict were considered by the steering assistance controller. Ref. [18] presented a novel shared control concept for lane keeping assist (LKA) systems of intelligent vehicles. The core idea is to combine system perception with robust control so that the proposed strategy can successfully share the control authority between human drivers and the LKA system. In [19,20], a novel weighted method is proposed to solve the conflict problem of shared control authority. Moreover, the author emphasized that the fictive control saturation about the steering angle can be easily reached even if the actuator did not reach its physical limitations. Therefore, the control input saturation should be considered in the controller design to prevent performance degradation.

Notably, the above research has mainly focused on the design of assistance controllers that consider control authority and driver characteristics, while less attention is paid to input saturation. Most research has only considered the saturation of the lateral force of the tire [21–24], and currently, there are only a few good methods to deal with the steering angle saturation [25]. In [25], a robust output feedback controller is presented to adjust the lateral vehicle dynamics under front lateral tire force saturation and a network delay. In [26], a robust yaw moment controller is proposed to improve vehicle stability by considering the uncertainty of the vehicle mass, moment of inertia, cornering stiffness, and control saturation. In [27], the Takagi–Sugeno (T-S) fuzzy method for nonlinear systems under the action of actuator saturation is proposed, and the problem of estimation of the attractive region of the T-S fuzzy system is given by the optimization method. In [28], based on the T-S fuzzy model, a lateral control method is described to address a new driver–automatic collaboration method for the lateral shared control of lane keeping assist systems (LKAS) devices. Under the design conditions based on the least squares method, the input saturation, the driver's safety, and comfort are clearly considered in the control design. Nevertheless, the lateral control method based on the T-S fuzzy model is proposed to implement control saturation. Moreover, penalizing the objective function so that the physical limits of the actuator are never reached often leads to weak and conservative designs [29]. Model predictive control (MPC) [30,31] is a very effective method for path following with the consideration of the steering angle saturation, but its complexity and less ability to deal with uncertainty are the main shortcomings. Compared with most existing anti-windup schemes, anti-windup [32–35] compensation schemes are less conservative, but their sizeable computational amount and complexity are the main shortcomings of these algorithm. Therefore, when disturbances and uncertainties are involved in a driver–vehicle system, the input saturation should be clearly considered to prevent performance

degradation and the loss of stability [36,37]. Moreover, it is crucial to deal with input saturation by considering a simple computation method.

Thus, this paper mainly considers how to design a simple and effective controller to assist drivers in improving driving performance and reducing workload by considering fictive control input saturation. Moreover, in [15], it was pointed out that the controller can reduce the lateral deviation by providing a larger assistance steering angle, especially for inexperienced drivers. Thus, the different drivers should be considered to obtain optimal driving performance by a different saturation threshold value of the control input. A gain scheduling output feedback controller taking into account time-varying driver parameters, vehicle dynamic parameters, and assistance control saturation is proposed in this paper, which can improve the convergence rate of the state [38]. A driver–vehicle system with uncertainties and disturbances is established by combining the vehicle dynamics model and the driver model. The driver–vehicle system mainly considers the uncertainties of driver parameters and tire stiffness to improve the robustness performance. A gain scheduling output feedback controller [39] is designed to assist the driver with the consideration of the input saturation. The simulation results, which are based on the MATLAB-CarSim co-simulation platform, show that the proposed controller can effectively support the driver in reducing the workload and lateral deviations. Additionally, the vehicles can effectively follow the trajectory.

The main structure of this article is grouped into the following parts: (1) This paper describes the modelling of the driver model and vehicle dynamics. (2) To improve the robustness performance of the driver–vehicle system, the uncertainties of the driver-vehicle system are developed, including the tire cornering stiffness at the front and rear, external disturbances, and driver parameters, including the preview time, steering gain and driver delay time. (3) The gain scheduling output feedback controller with saturation is applied to the driver–vehicle system to handle assistance angle saturation and uncertainties. (4) The CarSim/Simulink co-simulation platform is proposed to verify the effectiveness of the proposed method in changing lane maneuvers. (5) The simulation results are presented in Section 4.

2. System Modelling

In this section, the vehicle dynamics and the driver model are described. To ameliorate the robustness performance of the system, we take into account the uncertainties of the tire cornering stiffness, driver characteristic parameters, and system modelling. Moreover, the input saturation is considered by the gain scheduling output feedback controller.

2.1. Driver–Vehicle System

For the sake of designing the path following controller and considering vehicle dynamics, it is supposed that the slip angle and front steering angle of the vehicle are relatively small. Assuming that the vehicle state equation is linear, a two-degree bicycle dynamics model [40] with a linear parameter variation (LPV) is obtained by using the linear proportional relationship between the side angle and lateral tyre force. The path following model of intelligent vehicles is shown in Figure 1.

$$m\dot{V}_y = -mV_x\dot{\psi} + F_{yf} + F_{yr} \tag{1}$$

$$\ddot{\psi} = \frac{1}{I_z}\left(L_f F_{yf} - L_r F_{yr}\right) \tag{2}$$

$$\dot{Y} = V_x\psi + V_y \tag{3}$$

where m denotes the mass of the vehicle, I_z denotes the yaw moment of the inertia, F_{yf} denotes lateral tyre forces at the front, F_{yr} denotes the lateral tyre forces at the rear, L_f denotes the distances between the front axles and the CG of the vehicle, L_r denotes the distances between the rear axles and the CG, V_y denotes the lateral speed, V_x denotes the longitudinal speed, ψ denotes the yaw angle, and Y

denotes the lateral position of the CG along the global coordinates. The formula of the lateral tire force is expressed as

$$F_{yf} = -C_f \alpha_f \, , \, F_{yr} = -C_r \alpha_r \tag{4}$$

where C_f and C_r denote the front and rear tyre cornering stiffness, respectively, and α_f and α_r denote the front and rear slip angles of the tyre and are expressed as

$$\alpha_f = \frac{L_f \dot{\psi}}{V_x} + \frac{V_y}{V_x} - \delta_f \, , \, \alpha_r = \frac{V_y}{V_x} - \frac{L_r \dot{\psi}}{V_x} \tag{5}$$

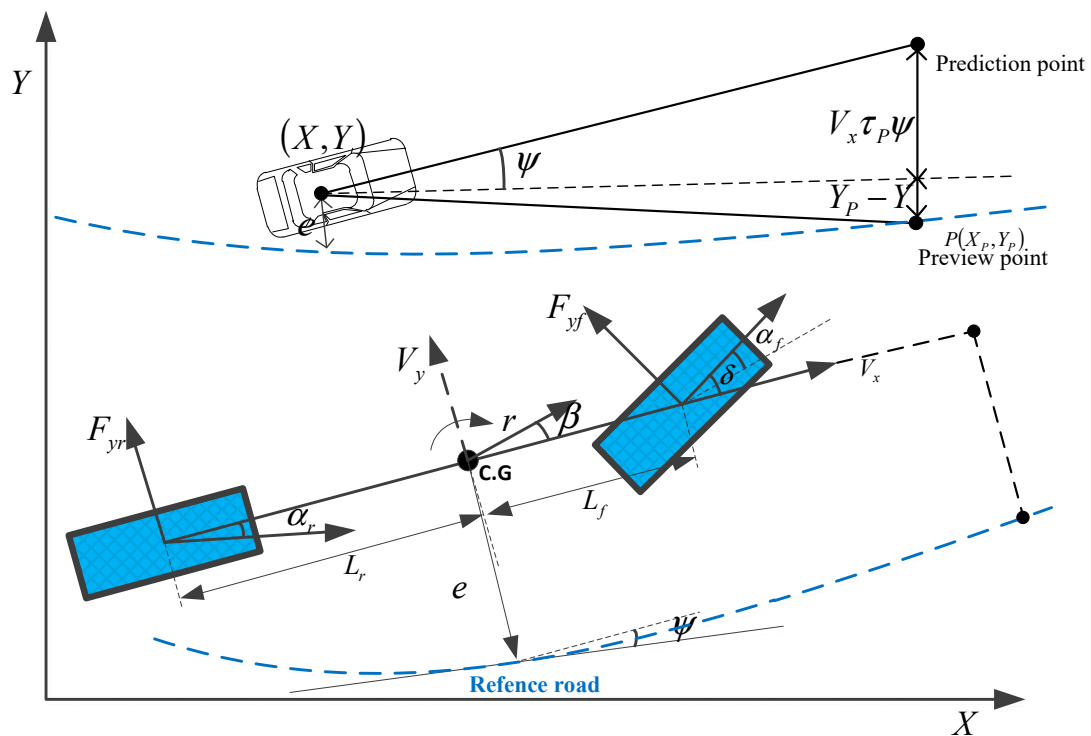where δ_f is the front wheel steering angle.

Figure 1. The path following the model of intelligent vehicles.

The parameter e is the lateral offset of the CG and can be expressed as

$$\dot{e} = V_x \psi + V_y \tag{6}$$

A fundamental driver model is used to minimize the lateral offset concerning the given reference road. As shown in Figure 1, the driver model [41,42] can be described as

$$\delta_d = \frac{G_d}{1 + \tau_d s} \left(Y_p - Y - V_x \tau_p \psi \right) \tag{7}$$

where G_d and τ_d are the steering gain and delay time of the driver, respectively, τ_p is the driver preview time, and Y_p is the lateral offset of the preview point. Based on the above driver model, the driver's steer parameters are estimated and obtained, by optimizing the parameters for the simulated driver's steer angle during a lane change to best agree with the actual/measured driver's steer angle obtained from the experimental tests [41]. Assuming that the road curvature is small, then $e \approx Y_p - Y$. According to [15],

$\delta_f = \delta_d + u$, and u is the designed assistance steering angle. Then, combining (1)–(7), the tracking trajectory system of the driver-vehicle can be described as

$$\dot{x} = A(t)x + B_1 d + B_2 u \qquad (8)$$

where x is the state variables of the path following model as $x = \begin{bmatrix} e & \dot{e} & \psi & \dot{\psi} & \delta_d \end{bmatrix}^T$, A is the system matrix, B_2 is the control matrix, d is the system disturbance vector, and B_1 is the disturbance matrix.

$$A(t) = \begin{bmatrix} 0 & 1 & 0 & 0 & 0 \\ 0 & \frac{C_f + C_r}{mV_x} & -\frac{C_f + C_r}{m} & \frac{C_f L_f - C_r L_r}{mV_x} & \frac{C_f}{m} \\ 0 & 0 & 0 & 1 & 0 \\ 0 & \frac{C_r L_r - C_f L_f}{I_z V_x} & \frac{C_r L_r - C_f L_f}{I_z} & -\frac{C_r L_r^2 + C_f L_f^2}{I_z V_x} & \frac{C_f L_f}{I_z} \\ \frac{G_d}{\tau_d} & 0 & -\frac{G_d \tau_p V_x}{\tau_d} & 0 & -\frac{1}{\tau_d} \end{bmatrix}$$

$$B_2(t) = \begin{bmatrix} 0 & \frac{C_f}{m} & 0 & \frac{C_f L_f}{I_z} & 0 \end{bmatrix}^T, \; B_1(t) = I, \; d = \begin{bmatrix} d_1 & d_2 & d_3 & d_4 & d_5 \end{bmatrix}^T$$

2.2. System Uncertainties

Human drivers have different driving characteristic parameters, which are the uncertainties in the driver–vehicle system. These driving characteristic parameters include the steering gain, preview time, and delay time and can be regarded as varying parameters. This paper mainly considers these varying parameters to be G_d, τ_p, and τ_d and assumes that there is a 5% uncertainty.

To simplify the uncertainties of the controller, according to [14], the characteristic parameters can be expressed as

$$\frac{1}{\tau_d} = \frac{1}{\tau_{d0}} + \theta_1 N_1 , \; \frac{G_d}{\tau_d} = \frac{G_{d0}}{\tau_{d0}} + \theta_2 N_2 , \; \frac{G_d \tau_p}{\tau_d} = \frac{G_{d0} \tau_{p0}}{\tau_{d0}} + \theta_3 N_3 \qquad (9)$$

where G_{d0} is the nominal value of the gain, τ_{p0} is the nominal value of the preview time, τ_{d0} is the nominal value of the delay, $\widetilde{G}_d$ is the uncertainty value of the gain, $\widetilde{\tau}_p$ is the uncertain value of the preview time, $\widetilde{\tau}_d$ is the uncertainty value of the delay, and θ_1, θ_2, and θ_3 are uncertainty values. N_1, N_2, and N_3 are the uncertainty coefficients and are expressed as

$$\theta_1 = \frac{1}{\widetilde{\tau}_d}$$

$$\theta_2 = \frac{G_{d0}}{\widetilde{\tau}_d} + \frac{\widetilde{G}_d}{\tau_{d0}} + \frac{\widetilde{G}_d}{\widetilde{\tau}_d} \qquad (10)$$

$$\theta_3 = \theta_3 \tau_{p0} + \frac{G_{d0}}{\tau_{d0}} \widetilde{\tau}_p + \frac{G_{d0}}{\widetilde{\tau}_d} \widetilde{\tau}_p + \frac{\widetilde{G}_d}{\tau_{d0}} \widetilde{\tau}_p + \frac{\widetilde{G}_d}{\widetilde{\tau}_d} \widetilde{\tau}_p$$

$$|N_i| < 1 \; i \epsilon \{1, 2, 3\} \qquad (11)$$

The tire cornering stiffness is mainly affected by the speed, the reasonable force, and the road, which are varying parameters. The tire cornering stiffness is considered to be an inaccurate parameter in the system and can be described by the following:

$$C_f = C_{f0} + N_f \widetilde{C}_f , \; C_r = C_{r0} + N_r \widetilde{C}_r \qquad (12)$$

Then, by combining Equations (8)–(12), the driver-vehicle system considering the uncertainties of the driving characteristic parameters and tire cornering stiffness is expressed as

$$\dot{x} = \left(\overline{A} + \Delta A \right)x + B_1 d + \left(\overline{B}_2 + \Delta B_2 \right)u \qquad (13)$$

where $A = \bar{A} + \Delta A$, $B_2 = \bar{B}_2 + \Delta B_2$, $\Delta A = \widetilde{A} N_A E$, $\Delta B = \widetilde{B}_2 N_B$.

Considering the saturated linear plant subject to actuator saturation, Equation (13) can be expressed as

$$
\begin{cases}
\dot{x} = Ax + B_1 d + B_2 sat(u) \\
e = C_1 x + D_{11} d + D_{12} sat(u) \\
y = C_2 x + D_{21} d
\end{cases}
\tag{14}
$$

where e is the performance output of the linear saturated plant, y is the measurement output, $sat(u)$ is the saturation function, and $\bar{u}$ is the maximum positive value of the control input.

$$
sat(u) = \begin{cases}
\bar{u} & u \geq \bar{u} \\
u & -\bar{u} \leq u \leq \bar{u} \\
-\bar{u} & u \leq -\bar{u}
\end{cases}
$$

3. Problem Formulation and Robust Controller Design

In this section, the design procedure of the controller is described in detail. The goal of the controller is to minimize the lateral offset relative to a given reference trajectory as soon as possible.

3.1. Problem Formulation

To consider the control saturation, the system Equation (14), which can be described in the form of a dead-zone function, can be expressed as

$$
\begin{bmatrix}
\dot{x} \\
u \\
e \\
y
\end{bmatrix}
=
\begin{bmatrix}
A & -B_2 & B_1 & B_2 \\
0 & 0 & 0 & I \\
C_1 & -D_{12} & D_{11} & D_{12} \\
C_2 & 0 & D_{21} & 0
\end{bmatrix}
\begin{bmatrix}
x \\
p \\
d \\
u
\end{bmatrix}
\tag{15}
$$

$$
p = dz(u)
\tag{16}
$$

where $dz(u) = u - sat(u)$ is the dead-zone function.

Consider a scheduling controller in the form of that described in Equations (17) and (18).

$$
\begin{bmatrix}
\dot{x}_k \\
q_k \\
u
\end{bmatrix}
=
\begin{bmatrix}
A_k & B_{k0} & B_{k1} \\
C_{k0} & D_{k00} & D_{k01} \\
C_{k1} & D_{k10} & D_{k11}
\end{bmatrix}
\begin{bmatrix}
x_k \\
p_k \\
y
\end{bmatrix}
\tag{17}
$$

$$
p_k = dz(q_k)
\tag{18}
$$

where x_k is the state matrix and p_k and q_k are the input and output of a scheduling controller, respectively.

According to Theorem 1 [38], Formulations (16) and (18) can be described as

$$
p = \Theta(u - H_2 x_k)
\tag{19}
$$

$$
p_k = \Theta(q_k - H_4 x_k)
\tag{20}
$$

where the parameter is limited to $0 \leq \Theta \leq 1$ here.

Theorem 1. *Let $h(x) = Hx$ be a linear relationship, and assume that $Hx \in [-\bar{u}, \bar{u}]$. For any u, we have $sat(u) \in Co\{u, Hx\}$ and $dz = \theta(u - Hx)$ for some $\theta \in [0,1]$.*

Then, by combining Formulations (15), (17), (19), and (20), the system is described as

$$
\begin{bmatrix} \dot{x}_{CL} \\ q_{CL} \\ e \end{bmatrix} = \begin{bmatrix} A_{CL} & B_{0,CL} & B_{1,CL} \\ C_{0,CL} & D_{00,CL} & D_{01,CL} \\ C_{1,CL} & D_{10,CL} & D_{11,CL} \end{bmatrix} \begin{bmatrix} x_{CL} \\ p_{CL} \\ d \end{bmatrix} \tag{21}
$$

$$
p_{CL} = \begin{bmatrix} \Theta & 0 \\ 0 & \Theta \end{bmatrix} (q_{CL} - Hx_{CL}) \tag{22}
$$

where $x_{CL} = \begin{bmatrix} x & x_k \end{bmatrix}^T q_{CL} = \begin{bmatrix} u & q_k \end{bmatrix}^T p_{CL} = \begin{bmatrix} p & p_k \end{bmatrix}^T$.

$$
\begin{bmatrix} A_{CL} & B_{0,CL} & B_{1,CL} \\ C_{0,CL} & D_{00,CL} & D_{01,CL} \\ C_{1,CL} & D_{10,CL} & D_{11,CL} \end{bmatrix} = \begin{bmatrix} A & 0 & -B_2 & 0 & B_1 \\ 0 & 0 & 0 & 0 & 0 \\ 0 & 0 & 0 & 0 & 0 \\ 0 & 0 & 0 & 0 & 0 \\ C_1 & 0 & -D_{12} & 0 & D_{11} \end{bmatrix} + \cdots \tag{23}
$$

$$
\cdots + \begin{bmatrix} 0 & B_2 & 0 \\ I & 0 & 0 \\ 0 & I & 0 \\ 0 & 0 & I \\ 0 & D_{12} & 0 \end{bmatrix} \begin{bmatrix} A_k & B_{k1} & B_{k0} \\ C_{k1} & D_{k11} & D_{k10} \\ C_{k0} & D_{k01} & D_{k00} \end{bmatrix} \begin{bmatrix} 0 & I & 0 & 0 & 0 \\ C_2 & 0 & 0 & 0 & D_{21} \\ 0 & 0 & 0 & I & 0 \end{bmatrix}
$$

$$
H = \begin{bmatrix} 0 & H_2 \\ 0 & H_4 \end{bmatrix} \Pi = \begin{bmatrix} A_k & B_{k1} & B_{k0} \\ C_{k1} & D_{k11} & D_{k10} \\ C_{k0} & D_{k01} & D_{k00} \end{bmatrix}
$$

3.2. Robust Controller Design

For trajectory tracking, it is necessary to find the controller to make the tracking error converge under the uncertainties of the parameters and disturbance. The structure of the proposed method is illustrated in Figure 2.
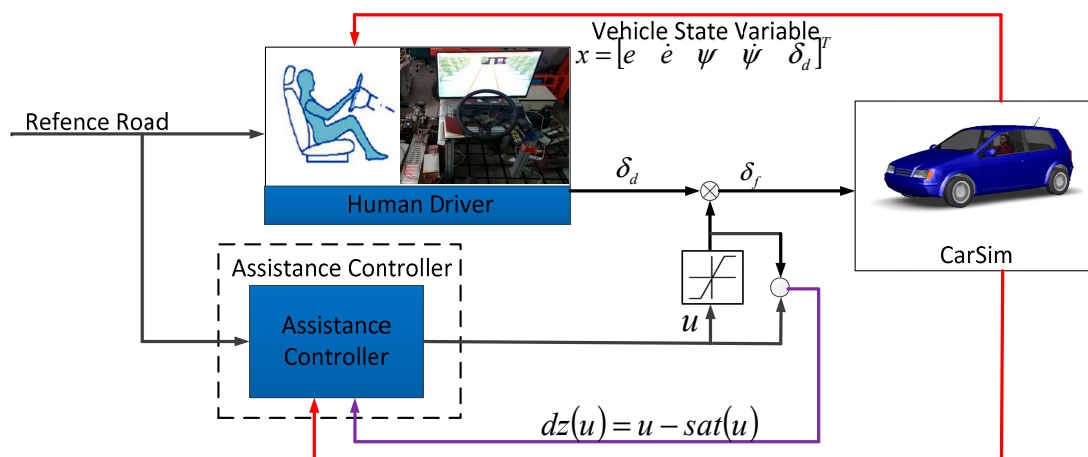

Figure 2. Structure of the proposed method.

According to a quadratic Lyapunov function $V = x_{CL}^T P x_{CL}$ and a matrix $\Lambda = diag(\Theta, \Theta) > 0$, the quadratic Lyapunov function of the system (21) and (22) can be described as

$$\dot{V} + \frac{1}{\gamma^2} e^T e + p_{CL}^T \Lambda (q_{CL} - p_{CL} - H x_{CL}) + (q_{CL} - p_{CL} - H x_{CL})^T \Lambda p_{CL} - d^T d < 0 \qquad (24)$$

Moreover, the actuator saturation set inclusion condition can be described as

$$\left\{ x_{CL} : x_{CL}^T P x_{CL} \leq s^2 \right\} \subset \left\{ x_{CL} : \left| \begin{bmatrix} 0 & H_2 \end{bmatrix} x_{CL} \right| \leq \bar{u} \right\} \qquad (25)$$

where given scalars $s > 0$, and a positive matrix P. According to the scaled bounded real lemma, (23) and (24) can be rewritten in the following form:

$$\begin{bmatrix} A_{CL}^T P + P A_{CL} & * & * & * \\ \Lambda(C_{0,CL} - H) + B_{0,CL}^T P & (D_{00,CL} - I)^T \Lambda + \Lambda(D_{00,CL} - I) & * & * \\ B_{1,CL}^T P & D_{01,CL}^T \Lambda & -I & * \\ C_{1,CL} & D_{10,CL} & D_{11,CL} & -\gamma^2 I \end{bmatrix} < 0 \qquad (26)$$

$$\begin{bmatrix} \frac{\bar{u}^2}{s^2} & \begin{bmatrix} 0 & H_2 \end{bmatrix} \\ \begin{bmatrix} 0 \\ H_2^T \end{bmatrix} & P \end{bmatrix} \geq 0 \qquad (27)$$

To improve system performance in the existence of the uncertainty of the parameters, disturbance, and input saturation, Theorem 2 is introduced in the following term.

Theorem 2. *Ref. [39]. For system (21) and (22), the control objectives in (23) and (24) are satisfied. The relation $s, \gamma > 0$ is given if there exist positive matrices R, S, positive diagonal matrices L, J and a rectangular matrix $\widetilde{H}_2$ such that*

$$\begin{bmatrix} H_{\tilde{\Phi}}^T & 0 \\ 0 & I \end{bmatrix} \begin{bmatrix} R(\bar{A} + \Delta A)^T + (\bar{A} + \Delta A)R & * & * & * \\ -L(\bar{B}_2 + \Delta B_2)^T - \widetilde{H}_2 & -2L & * & * \\ C_1 R & -D_{12}L & -\gamma^2 I & * \\ B_1^T & 0 & D_{11}^T & -I \end{bmatrix} \begin{bmatrix} H_{\tilde{\Phi}} & 0 \\ 0 & I \end{bmatrix} < 0 \qquad (28)$$

$$\begin{bmatrix} H_{\Gamma}^T & 0 \\ 0 & I \end{bmatrix} \begin{bmatrix} (\bar{A} + \Delta A)^T S + S(\bar{A} + \Delta A) & * & * & * \\ B_1^T S & -I & * & * \\ -(\bar{B}_2 + \Delta B_2)^T S & 0 & -2J & * \\ C_1 & D_{11} & -D_{12} & -\gamma^2 I \end{bmatrix} \begin{bmatrix} H_{\Gamma} & 0 \\ 0 & I \end{bmatrix} < 0 \qquad (29)$$

$$\begin{bmatrix} R & I \\ I & S \end{bmatrix} > 0 \qquad (30)$$

$$\begin{bmatrix} L & I \\ I & J \end{bmatrix} > 0 \qquad (31)$$

$$\begin{bmatrix} \frac{\bar{u}^2}{s^2} & \widetilde{H}_2 & 0 \\ * & R & I \\ * & * & S \end{bmatrix} > 0 \qquad (32)$$

where

$$H_{\widetilde{\Phi}} = \left[\; H_{\Phi_1}^T \quad H_{\Phi_2}^T \quad H_{\widetilde{\Phi}_3}^T \;\right]^T = Ker\left[\; B_2^T \quad I \quad D_{12}^T \;\right] H_{\Gamma} = \left[\; H_{\Gamma_1}^T \quad H_{\Gamma_2}^T \;\right]^T = Ker\left[\; C_2 \quad D_{21} \;\right].$$

The above feasibility problem is transformed into an optimization problem, which is described as

$$\begin{array}{c} Min\ \gamma^2 \\ subj.to\,(27) - (31) \end{array} \tag{33}$$

For systems (21) and (22), the control objectives in (23) and (24) are satisfied by using Theorem 2 and calculating the above linear matrix inequality (LMI). The proof of Theorem 2 can be found in [39] and is thus ignored here. Obviously, Theorem 2 cannot directly solve the scheduling controller. However, Inequality (25) can be applied to solve the value of a scheduling controller again. By combining the LMI (25) and Equation (21), the inequality can be simplified and rewritten as

$$\Psi_0 + \alpha^T H_4 \beta + \beta^T H_4^T \alpha + \Gamma^T \Pi^T \Phi + \Phi^T \Pi \Gamma < 0 \tag{34}$$

Based on the Inequality (33), the controller gain can be obtained by calculating Π and H_4 by solving the LMI feasibility problem.

The matrix $R, S, L, J, \widetilde{H}_2$ can be calculated by making use of the Theorem 2, and the matrix $M, N, U, V, \mathcal{R}_3, H_2$ can be obtained by choosing suitable matrices such that $UV^T = I - LJ$, $MN^T = I - RS$, determining $\mathcal{R}_3$ form the constructed Λ matrix and computing $H_2 = \widetilde{H}_2 (M^T)^{-1}$.

$$\Psi_0 = \begin{bmatrix} (\overline{A} + \Delta A)^T S + S(\overline{A} + \Delta A) & * & * & * & * & * \\ N^T A & 0 & * & * & * & * \\ -(\overline{B}_2 + \Delta B_2)^T S & -(\overline{B}_2 + \Delta B_2)^T N - JH_2 & -2J & * & * & * \\ 0 & -V^T H_2 & -2V^T & -2\mathcal{R}_3 & * & * \\ B_1^T S & B_1^T N & 0 & 0 & -I & * \\ C_1 & 0 & -D_{12} & 0 & D_{11} & -\gamma^2 I \end{bmatrix}.$$

$$P = \begin{bmatrix} S & N \\ N^T & \mathcal{R}_1 \end{bmatrix} P^{-1} = \begin{bmatrix} R & M \\ M^T & \mathcal{R}_2 \end{bmatrix} \Lambda = \begin{bmatrix} J & V \\ V^T & \mathcal{R}_3 \end{bmatrix} \Lambda^{-1} = \begin{bmatrix} L & U \\ U^T & \mathcal{R}_4 \end{bmatrix}$$

$$F_1 = \begin{bmatrix} 0 & I \\ C_2 & 0 \\ 0 & 0 \end{bmatrix} F_2 = \begin{bmatrix} 0 & 0 \\ 0 & 0 \\ 0 & 1 \end{bmatrix} F_3 = \begin{bmatrix} 0 \\ D_{21} \\ 0 \end{bmatrix}$$

$$G_1 = \begin{bmatrix} 0 & B_2 & 0 \\ I & 0 & 0 \end{bmatrix} G_2 = \begin{bmatrix} 0 & I & 0 \\ 0 & 0 & I \end{bmatrix} G_3 = \begin{bmatrix} 0 & D_{12} & 0 \end{bmatrix}$$

$$\Gamma = \begin{bmatrix} F_1 & F_2 & F_3 & 0 \end{bmatrix} \Phi = \begin{bmatrix} G_1^T P & G_2^T \Lambda & 0 & G_3^T \end{bmatrix}$$

$$\alpha = \begin{bmatrix} 0 & 0 & -V^T & -\mathcal{R}_3^T & 0 & 0 \end{bmatrix} \beta = \begin{bmatrix} 0 & I & 0 & 0 & 0 & 0 \end{bmatrix}$$

In summary, we take advantage of Theorem 2 to calculate the matrix $R, S, L, J, \widetilde{H}_2$ by solving the LMI optimization problem. Then, the gain Π can be obtained by solving the LMI feasibility problem for Inequality (33).

Theorem 2 and Inequality (33), which contain the time-varying parameters N_A, N_B, cannot be applied to the controller design directly. Therefore, to address uncertainties, Theorem 3 is derived and described as follows.

Theorem 3. *For system (21) and (22), the controller performance in (23) and (24) is satisfied. The scalars* $s, \gamma, \varepsilon > 0$ *are given if there exist positive diagonal matrices L, J, positive matrices R, S, and a rectangular matrix* $\widetilde{H}_2$ *such that*

$$
\begin{bmatrix}
\ell_1^T \Omega_1 \ell_1 & \varepsilon \ell_1^T \mathfrak{I}_{11} & \ell_1^T \mathfrak{I}_{12}^T \\
* & -\varepsilon I & 0 \\
* & * & -\varepsilon I
\end{bmatrix} < 0
\tag{35}
$$

$$
\begin{bmatrix}
\ell_2^T \Omega_2 \ell_2 & \varepsilon \ell_2^T \mathfrak{I}_{21} & \ell_2^T \mathfrak{I}_{22}^T \\
* & -\varepsilon I & 0 \\
* & * & -\varepsilon I
\end{bmatrix} < 0
\tag{36}
$$

$$
\begin{bmatrix}
R & I \\
I & S
\end{bmatrix} > 0
\tag{37}
$$

$$
\begin{bmatrix}
L & I \\
I & J
\end{bmatrix} > 0
\tag{38}
$$

$$
\begin{bmatrix}
\frac{\bar{u}^2}{s^2} & \widetilde{H}_2 & 0 \\
* & R & I \\
* & * & S
\end{bmatrix} > 0
\tag{39}
$$

Proof. The uncertainty terms of Equation (13) can be expressed as

$$
\Delta A = \widetilde{A} N_A E \quad \Delta B = \widetilde{B}_2 N_B
\tag{40}
$$

where

$$
N_A = diag\begin{pmatrix} N_1 & N_f & N_r & N_f & N_r & N_2 & N_f & N_r & N_f & N_3 \end{pmatrix}
$$

$$
\widetilde{A} = \begin{bmatrix}
0 & 0 & 0 & 0 & 0 & 0 & 0 & 0 & 0 & 0 \\
0 & \frac{\widetilde{C}_f}{mV_x} & \frac{\widetilde{C}_r}{mV_x} & -\frac{\widetilde{C}_f}{m} & -\frac{\widetilde{C}_r}{m} & 0 & \frac{L_f\widetilde{C}_f}{mV_x} & -\frac{L_r\widetilde{C}_r}{mV_x} & \frac{\widetilde{C}_f}{m} & 0 \\
0 & 0 & 0 & 0 & 0 & 0 & 0 & 0 & 0 & 0 \\
0 & -\frac{L_f\widetilde{C}_f}{I_zV_x} & \frac{L_r\widetilde{C}_r}{I_zV_x} & -\frac{L_f\widetilde{C}_f}{I_z} & \frac{L_r\widetilde{C}_r}{I_z} & 0 & -\frac{L_f^2\widetilde{C}_f}{I_zV_x} & -\frac{L_r^2\widetilde{C}_f}{I_zV_x} & \frac{L_f\widetilde{C}_f}{I_z} & 0 \\
\frac{G_{d0}}{\tau_{d0}} & 0 & 0 & 0 & 0 & -\frac{G_{d0}\tau_{p0}V_x}{\tau_{d0}} & 0 & 0 & 0 & -\frac{1}{\tau_{d0}}
\end{bmatrix}
$$

$$
\widetilde{B}_2 = \begin{bmatrix} 0 \\ \frac{\widetilde{C}_f}{m} \\ 0 \\ \frac{L_f\widetilde{C}_f}{I_z} \\ 0 \end{bmatrix}
\quad
E = \begin{bmatrix}
1 & 0 & 0 & 0 & 0 \\
0 & 1 & 0 & 0 & 0 \\
0 & 1 & 0 & 0 & 0 \\
0 & 0 & 1 & 0 & 0 \\
0 & 0 & 1 & 0 & 0 \\
0 & 0 & -V_x & 0 & 0 \\
0 & 0 & 0 & 1 & 0 \\
0 & 0 & 0 & 1 & 0 \\
0 & 0 & 0 & 0 & 1 \\
0 & 0 & 0 & 0 & -1
\end{bmatrix}
$$

Considering the Equality (39), the Theorem 2 Inequalities (27) and (28) can be further rewritten as

$$
\ell_1^T \left(\Omega_1 + \mathfrak{I}_{11} \aleph \mathfrak{I}_{12} + \mathfrak{I}_{12}^T \aleph^T \mathfrak{I}_{11}^T \right) \ell_1 < 0
\tag{41}
$$

$$
\ell_2^T \left(\Omega_2 + \mathfrak{I}_{21} \aleph \mathfrak{I}_{22} + \mathfrak{I}_{22}^T \aleph^T \mathfrak{I}_{21}^T \right) \ell_2 < 0
\tag{42}
$$

where

$$
\Omega_1 = \begin{bmatrix} R\overline{A}^T + \overline{A}R & * & * & * \\ -L\overline{B}_2^T - \widetilde{H}_2 & -2L & * & * \\ C_1 R & -D_{12}L & -\gamma^2 I & * \\ B_1^T & 0 & D_{11}^T & -I \end{bmatrix}
\quad
\Omega_2 = \begin{bmatrix} \overline{A}^T S + S\overline{A} & * & * & * \\ B_1^T S & -I & * & * \\ -\overline{B}_2^T S & 0 & -2J & * \\ C_1 & D_{11} & -D_{12} & -\gamma^2 I \end{bmatrix}
$$

$$
\mathfrak{I}_{11} = \begin{bmatrix} \widetilde{A} & -\widetilde{B} \\ 0 & 0 \\ 0 & 0 \\ 0 & 0 \end{bmatrix}
\quad
\mathfrak{I}_{12} = \begin{bmatrix} ER & 0 & 0 & 0 \\ 0 & L^T & 0 & 0 \end{bmatrix}
\quad
\ell_1 = \begin{bmatrix} H_{\widetilde{\Phi}} & 0 \\ 0 & I \end{bmatrix}
\quad
\aleph = \begin{bmatrix} N_A & 0 \\ 0 & N_B \end{bmatrix}
$$

$$
\mathfrak{I}_{12} = \begin{bmatrix} S\widetilde{A} & -S\widetilde{B} \\ 0 & 0 \\ 0 & 0 \\ 0 & 0 \end{bmatrix}
\quad
\mathfrak{I}_{22} = \begin{bmatrix} E & 0 & 0 & 0 \\ 0 & 0 & I & 0 \end{bmatrix}
\quad
\ell_1 = \begin{bmatrix} H_{\Gamma} & 0 \\ 0 & I \end{bmatrix}
$$

Then, by using [43] (Lemma2) and [15] (Lemma2), the Inequalities (40) and (41) is equivalent to the Inequalities (42) and (43). Thus, this completes the proof. □

$$
\begin{bmatrix} \ell_1^T \Omega_1 \ell_1 & \varepsilon \ell_1^T \mathfrak{I}_{11} & \ell_1^T \mathfrak{I}_{12}^T \\ * & -\varepsilon I & 0 \\ * & * & -\varepsilon I \end{bmatrix} < 0
\tag{43}
$$

$$
\begin{bmatrix} \ell_2^T \Omega_2 \ell_2 & \varepsilon \ell_2^T \mathfrak{I}_{21} & \ell_2^T \mathfrak{I}_{22}^T \\ * & -\varepsilon I & 0 \\ * & * & -\varepsilon I \end{bmatrix} < 0
\tag{44}
$$

Obviously, Theorem 3 is applied to calculate the matrix $R, S, L, J, \widetilde{H}_2$ by solving the LMI optimization problem. However, the gain Π of the controller cannot be calculated directly. It's worth noting that the matrix parameters $R, S, L, J, \widetilde{H}_2$ have already been calculated by using Theorem 3 Therefore, by making use of Inequality (33), which contains the matrix $R, S, L, J, \widetilde{H}_2$ and the gain Π, the gain Π of the controller can be calculated indirectly.

In the same way, by considering the Equality (39), then the Inequality (33) can be further described and rewritten as:

$$
\Omega_\Psi + \mathfrak{I}_{\Psi1} \aleph \mathfrak{I}_{\Psi2} + \mathfrak{I}_{\Psi2}^T \aleph^T \mathfrak{I}_{\Psi1}^T + \alpha^T H_4 \beta + \beta^T H_4^T \alpha + \Gamma^T \Pi^T \Phi + \Phi^T \Pi \Gamma < 0
\tag{45}
$$

Making use of [15] (Lemma2) to address uncertainties, Inequality (44) is further described as

$$
\begin{bmatrix} \Omega_\Psi + \alpha^T H_4 \beta + \beta^T H_4^T \alpha + \Gamma^T \Pi^T \Phi + \Phi^T \Pi \Gamma & \varepsilon \mathfrak{I}_{\Psi1} & \mathfrak{I}_{\Psi2}^T \\ * & -\varepsilon I & 0 \\ * & * & \varepsilon I \end{bmatrix} < 0
\tag{46}
$$

where

$$
\Omega_\Psi = \begin{bmatrix}
\overline{A}^T S + S\overline{A} & * & * & * & * & * \\
N^T A & 0 & * & * & * & * \\
-\overline{B}_2^T S & -\overline{B}_2^T N - J H_2 & -2J & * & * & * \\
0 & -V^T H_2 & -2V^T & -2\Re_3 & * & * \\
B_1^T S & B_1^T N & 0 & 0 & -I & * \\
C_1 & 0 & -D_{12} & 0 & D_{11} & -\gamma^2 I
\end{bmatrix}
\tag{47}
$$

$$\mathfrak{I}_{\Psi 1} = \begin{bmatrix} S\widetilde{A} & -S^T\widetilde{B}_2 \\ 0 & -N^T\widetilde{B}_2 \\ 0 & 0 \\ 0 & 0 \\ 0 & 0 \\ 0 & 0 \\ 0 & 0 \end{bmatrix} \quad \mathfrak{I}_{\Psi 2} = \begin{bmatrix} E & 0 & 0 & 0 & 0 \\ 0 & 0 & I & 0 & 0 \end{bmatrix}$$

To solve the scheduling controller Π, there is a need for more steps to calculate parameters. Firstly, Theorem 3 is applied to calculate the matrix $R, S, L, J, \widetilde{H}_2$ by solving the LMI optimization problem. Secondly, the known parameters $R, S, L, J, \widetilde{H}_2$ need to be substituted into the inequality. The gain Π of the controller can be obtained by solving the LMI feasibility problem for Inequality (45).

4. Simulation Results

The simulation is implemented on the CarSim-Simulink co-simulation platform. The LMI optimization problem can be solved by using the MATLAB Robust Control Toolbox. The vehicle dynamics parameters are listed as follows: $m = 1800$ kg, $I_z = 1600$ kg·m^2, $L_f = 1.3$ m, $L_r = 1.4$ m, $C_f = 80{,}000$ N/rad, and $C_r = 90{,}000$ N/rad. A comparison of the different drivers is made to highlight the advantages of the proposed approach, which help drivers reduce their workload and improve their driving performance. The driver A parameters are listed as follows.

$G_{d0} = 0.6$, $\tau_{p0} = 0.68$, $\tau_{d0} = 0.30$, $\widetilde{G}_d = 5\%{*}G_{d0}$, $\widetilde{\tau}_p = 5\%{*}\tau_{p0}$, and $\widetilde{\tau}_d = 5\%{*}\tau_{d0}$.

The assistance control saturation value is $\bar{u} = 10/180{*}3.14$.

The driver B parameters are listed as follows.

$G_{d0} = 0.7$, $\tau_{p0} = 0.68$, $\tau_{d0} = 0.23$, $\widetilde{G}_d = 5\%{*}G_{d0}$, $\widetilde{\tau}_p = 5\%{*}\tau_{p0}$, and $\widetilde{\tau}_d = 5\%{*}\tau_{d0}$.

The assistance control saturation value is $\bar{u} = 8/180{*}3.14$.

In the simulation, the vehicle is supposed to complete lane changing maneuvers with a constant vehicle speed of 20 m/s, which is proposed to complete the effectiveness verification of the proposed method. To evaluate controller performance, the driver average angle is defined and expressed as

$$w = \frac{\int_{t=0}^{t=T} |\delta_d| dt}{T}$$

4.1. Driver A Steering Manoeuvres Tests

The global trajectories are shown in Figure 3. The driver steering maneuvers without an assistance controller reach the largest lateral deviations at 85 m, and their global trajectory positions settle down at approximately 142 m. Meanwhile, the global trajectory position of the driver steering maneuvers with the controller converges at 130 m. Obviously, the controller can assist the driver by quickly reducing the lateral deviations and the overshoot. Notably, the controller with a consideration of the saturation converges faster than the controller without a consideration of the saturation.

The simulation results for the heading angle deviation, lateral deviation, lateral acceleration, and yaw rate are plotted in Figure 4. The maximum lateral deviation and heading deviation reach 0.23 m and 0.051 rad, respectively, when using the designed controller, which is smaller than that without the controller. Meanwhile, the lateral acceleration and yaw rate responses of the vehicle without the controller have larger amplitudes than the vehicle with the controller. This finding shows that the designed controller assists the driver in obtaining better driving performance. Compared with both controllers, the controller with a consideration of saturation has a small lateral deviation. The lateral acceleration and yaw rate with a consideration of saturation have slightly larger amplitudes than those without considering saturation. This result shows that the controller with a consideration of saturation can optimize the driving performance by limiting the input.
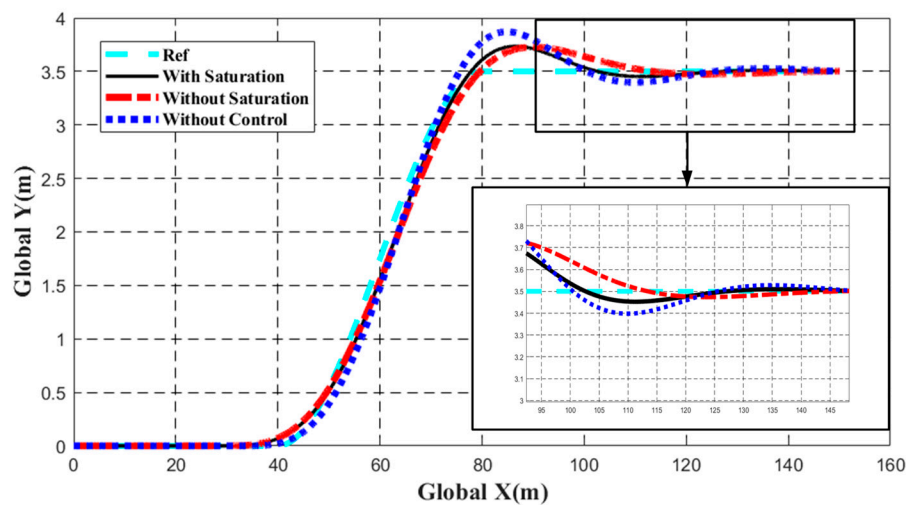
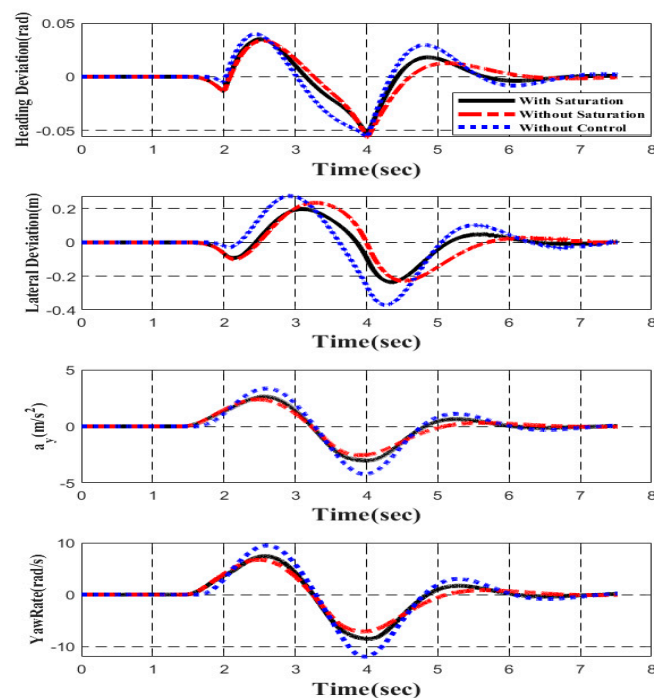**Figure 3.** The simulation results for the global trajectories.

Figure 4. The simulation results for the heading angle deviation, lateral deviation, lateral acceleration, and yaw rate.

The simulation results for the steering angle are plotted in Figure 5. The total steering angle of the drivers without the controller is larger than that with the controller and may lead to a potential lane departure. The result shows that the controller provides an assistance angle to help drivers traverse the trajectory.

The simulation results for the driver steering angle are plotted in Figure 6. It is clear that drivers without assistance control require more aggressive steering control angles to smoothly track the trajectory. The steering angle without using the controller is up to 44° at 3.8 s, and the driver suffers from driver overload. According to Table 1, the assistance controller provides a small assistance steering angle to assist the driver and can reduce the driver's workload. Moreover, the controller with the consideration of saturation can optimize driving performance and improve the state convergence rate by limiting the input.
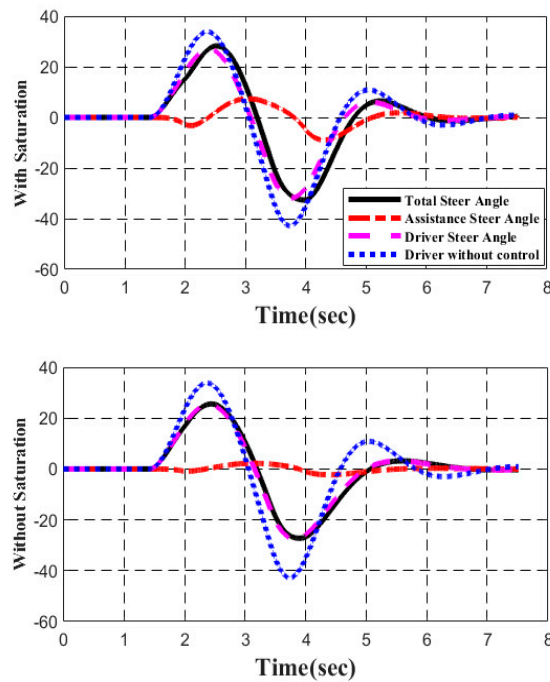
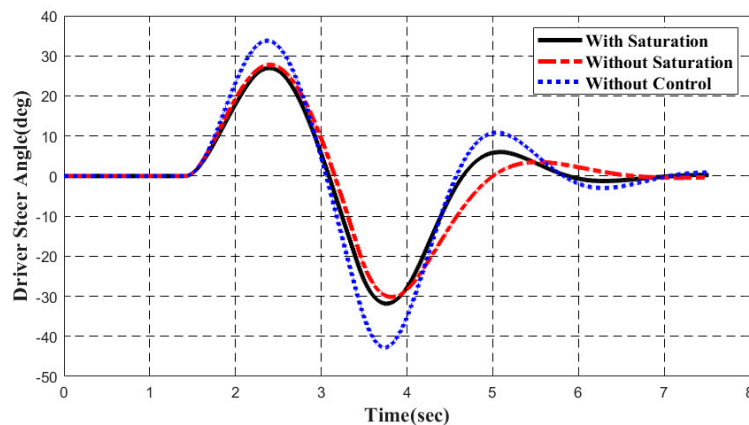**Figure 5.** The simulation results for the steer angle.

Figure 6. The simulation results for the driver steering angle.

Table 1. Driver average angle.

Controller Name	Driver Average Steer (°)
Driver 1 With Saturation	60.4275
Driver 1 Without Saturation	61.3871
Driver 1 Without Controller	80.0831

4.2. Driver B Steering Manoeuvre Tests

The global trajectories are shown in Figure 7. The driver maneuvers without using the controller have the largest lateral deviations at 90 m and tend to overshoot. The global trajectory position converges at 140 m. Meanwhile, the controller can help the driver quickly reduce the overshoot, and its global trajectories converge at 132 m, which is smaller than the trajectories without the help of the controller. Obviously, the controller can quickly assist the driver in reducing lateral deviations and the

overshoot. Compared with both controllers, the controller with consideration of saturation converges faster than the controller without consideration of saturation.

In Figure 8, the lateral deviation and the yaw deviation reach 0.51 m and 0.07 rad, respectively, at approximately 4.2 s without using the proposed controller, which may lead to a potential deterioration of the control accuracy. Meanwhile, the lateral acceleration and the yaw rate reach 3.8 m/s^2 and 10°/s, respectively. On the other hand, the lateral deviation and yaw deviation are maintained in the region of approximately 0.31 m and 0.065 rad, respectively. The lateral acceleration and the yaw rate of the vehicle with the controller can be kept in a range of 3.0 m/s^2 and 8°/s. This result shows that the designed controller assists the driver in obtaining better driving performance. Compared with both controllers, the controller with consideration of saturation has a smaller lateral deviation than that without saturation. The state convergence rate of the drive vehicle system can be improved by using the controller with the consideration of input saturation.
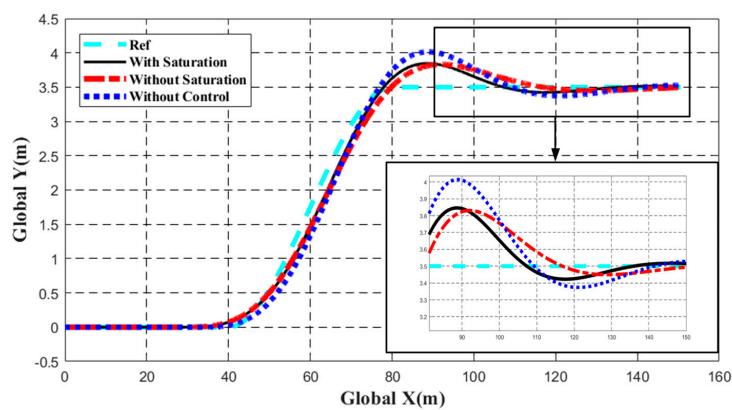

Figure 7. The simulation results for the global trajectories.
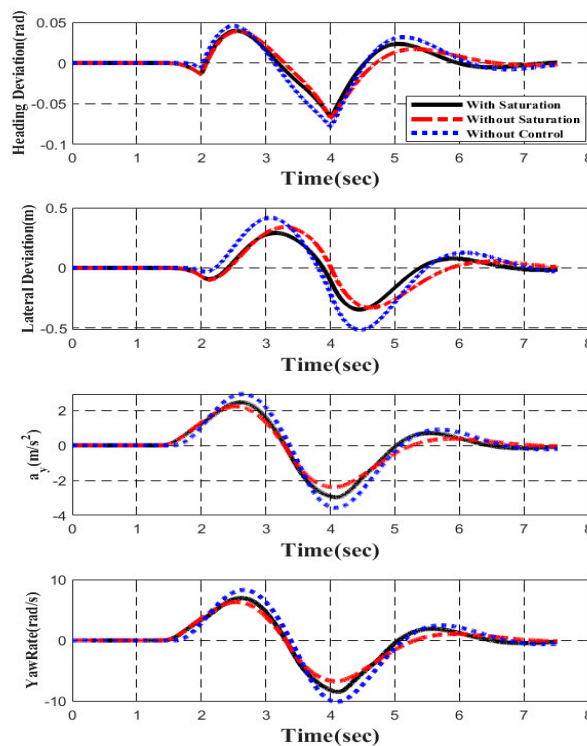

Figure 8. The simulation results for the heading angle deviation, lateral deviation, lateral acceleration, and yaw rate.

The simulation results for the steering angle are plotted in Figure 9. The total steering angle of drivers without the controller is larger than that with the controller and reaches 39° at 3.8 s, which may lead to a potential deterioration of the control accuracy and a large deviation from the given reference trajectory. Moreover, the controller provides an assistance angle to help the driver effectively follow the given trajectory.
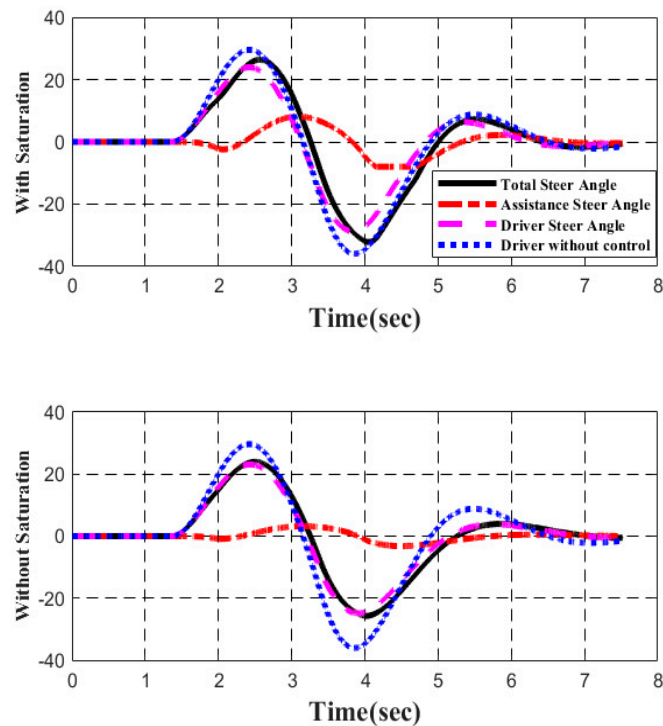

Figure 9. The simulation results for the steering angle.

The simulation results for the driver steer angle are shown in Figure 10. It is clear that the driver without a controller requires more aggressive steering control angles to smoothly track the given trajectory, which may lead to a large deviation. The steering angle without using the controller reaches 39° at 3.8 s and tends to overshoot. The driver steering angle using the designed controller can be maintained within a specific range of approximately 30°. According to Table 2, the assistance controller can reduce the driver's workload by providing a small assistance steering angle to assist the driver.
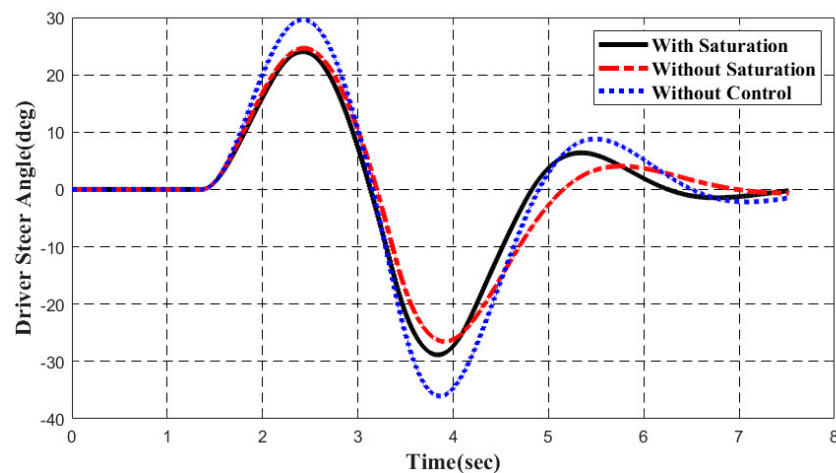

Figure 10. The simulation results for the driver steering angle.

Table 2. Driver average angle.

Controller Name	Driver Average Steer (°)
Driver 2 With Saturation	59.9365
Driver 2 Without Saturation	60.1861
Driver 2 Without Controller	77.7396

By analyzing the different steering maneuvers, different drivers have different driving characteristics in the absence of an assistance controller. The proposed controller can assist the drivers in reducing the workload and lateral deviation. The controller with saturation can further optimize driving performance and improve the state convergence rate by limiting the input.

5. Conclusions

In this paper, gain scheduling output feedback control for vehicle path tracking considering assistance steering saturation is proposed to assist drivers in tracking reference trajectories. Driver–vehicle modelling considers the uncertainties of the different driver parameters, tire cornering stiffness, and assistance steer angle saturation. A Lyapunov function considering saturation and uncertainty parameters is used to optimize the controller performance. Based on the MATLAB-CarSim co-simulation platform, the controller with saturation can reduce the steering workload and lateral deviation and improve the convergence rate of the state.

Author Contributions: Conceptualization, C.L. and W.Z.; Methodology, C.L., W.Z., and J.L.; Validation, W.Z. and J.L.; Formal analysis, W.Z., C.L., and J.L.; Investigation, C.L., J.L., and W.Z.; Data curation J.L. and C.L.; Writing—original draft preparation, C.L. and W.Z.; Writing—review and editing, W.Z., C.L., and J.L. All authors have read and agreed to the published version of the manuscript.

Conflicts of Interest: The authors declare no conflict of interest.

References

1. Alvarez, S.; Page, Y.; Sander, U.; Fahrenkrog, F.; Helmer, T.; Jung, O.; Hermitte, T.; Düering, M.; Döering, S.; Camp, O.O.D. Prospective effectiveness assessment of ADAS and active safety systems via virtual simulation: A review of the current practices. In Proceedings of the 25th International Technical Conference on the Enhanced Safety of Vehicles (ESV): Innovations in Vehicle Safety: Opportunities and Challenges, Detroit, MI, USA, 5–8 June 2017.
2. Auckland, R.A.; Manning, W.J.; Carsten, O.M.; Jamson, A.H. Advanced driver assistance systems: Objective and subjective performance evaluation. *Veh. Syst. Dyn.* **2008**, *46*, 883–897. [CrossRef]
3. Mulder, M.; Abbink, D.A.; Boer, E.R. Sharing Control with Haptics: Seamless Driver Support from Manual to Automatic Control. *Hum. Factors J. Hum. Factors Ergon. Soc.* **2012**, *54*, 786–798. [CrossRef] [PubMed]
4. Hasenjäger, M.; Heckmann, M.; Wersing, H. A Survey of Personalization for Advanced Driver Assistance Systems. *IEEE Trans. Intell. Veh.* **2020**, *5*, 335–344. [CrossRef]
5. Li, G.; Li, S.E.; Cheng, B. Field operational test of advanced driver assistance systems in typical Chinese road conditions: The influence of driver gender, age and aggression. *Int. J. Automot. Technol.* **2015**, *16*, 739–750. [CrossRef]
6. Martinez, C.M.; Heucke, M.; Wang, F.-Y.; Gao, B.; Cao, D. Driving Style Recognition for Intelligent Vehicle Control and Advanced Driver Assistance: A Survey. *IEEE Trans. Intell. Transp. Syst.* **2018**, *19*, 666–676. [CrossRef]
7. Wang, W.; Zhao, D.; Xi, J.; Leblanc, D.J.; Hedrick, J.K. Development and evaluation of two learning-based personalized driver models for car-following behaviors. In Proceedings of the 2017 American Control Conference (ACC), Seattle, WA, USA, 24–26 May 2017; pp. 1133–1138.

8. Weiss, E.; Thiel, M.F.; Sultana, N.; Hannan, C.; Seacrist, T. Advanced driver assistance systems for teen drivers: Teen and parent impressions, perceived need, and intervention preferences. *Traffic Inj. Prev.* **2018**, *19*, S120–S124. [CrossRef]

9. Petermeijer, S.; Abbink, D.A.; Mulder, M.; De Winter, J. The Effect of Haptic Support Systems on Driver Performance: A Literature Survey. *IEEE Trans. Haptics* **2015**, *8*, 467–479. [CrossRef]

10. Schnelle, S.; Wang, J.; Jagacinski, R.; Su, H.-J. A feedforward and feedback integrated lateral and longitudinal driver model for personalized advanced driver assistance systems. *Mechatronics* **2018**, *50*, 177–188. [CrossRef]

11. Minoiu-Enache, N.; Mammar, S.; Glaser, S.; Lusetti, B. Driver assistance system for lane departure avoidance by steering and differential braking. *IFAC Proc. Vol.* **2010**, *43*, 471–476. [CrossRef]

12. Németh, B.; Gáspár, P.; Bokor, J.; Sename, O.; Dugard, L. Fault-tolerant control design for trajectory tracking in driver assistance systems. *IFAC Proc. Vol.* **2012**, *45*, 186–191. [CrossRef]

13. Yih, P.; Gerdes, J.C. Modification of vehicle handling characteristics via steer-by-wire. *IEEE Trans. Control Syst. Technol.* **2005**, *13*, 965–976. [CrossRef]

14. Chen, Y.; Zhang, X.; Wang, J. Robust Vehicle Driver Assistance Control for Handover Scenarios Considering Driving Performances. *IEEE Trans. Syst. Man Cybern. Syst.* **2020**, 1–11. [CrossRef]

15. Wang, J.; Zhang, G.; Wang, R.; Schnelle, S.; Wang, J. A Gain-Scheduling Driver Assistance Trajectory-Following Algorithm Considering Different Driver Steering Characteristics. *IEEE Trans. Intell. Transp. Syst.* **2016**, *18*, 1097–1108. [CrossRef]

16. Sentouh, C.; Soualmi, B.; Popieul, J.-C.; Debernard, S. Cooperative Steering Assist Control System. In Proceedings of the 2013 IEEE International Conference on Systems Man and Cybernetics, Manchester, UK, 13–16 October 2013; pp. 941–946.

17. Sentouh, C.; Debernard, S.; Popieul, J.; Vanderhaegen, F. Toward a Shared Lateral Control Between Driver and Steering Assist Controller. *IFAC Proc. Vol.* **2010**, *43*, 404–409. [CrossRef]

18. Sentouh, C.; Nguyen, A.-T.; Benloucif, M.A.; Popieul, J.-C. Driver-Automation Cooperation Oriented Approach for Shared Control of Lane Keeping Assist Systems. *IEEE Trans. Control Syst. Technol.* **2019**, *27*, 1962–1978. [CrossRef]

19. Nguyen, A.-T.; Sentouh, C.; Popieul, J.-C.; Soualmi, B. Shared lateral control with on-line adaptation of the automation degree for driver steering assist system: A weighting design approach. In Proceedings of the 2015 54th IEEE Conference on Decision and Control (CDC), Osaka, Japan, 15–18 December 2015; pp. 857–862.

20. Nguyen, A.-T.; Sentouh, C.; Popieul, J.-C. Sensor Reduction for Driver-Automation Shared Steering Control via an Adaptive Authority Allocation Strategy. *IEEE/ASME Trans. Mechatron.* **2018**, *23*, 5–16. [CrossRef]

21. Hu, C.; Wang, R.; Yan, F.; Karimi, H.R. Robust Composite Nonlinear Feedback Path-Following Control for Independently Actuated Autonomous Vehicles With Differential Steering. *IEEE Trans. Transp. Electrif.* **2016**, *2*, 312–321. [CrossRef]

22. Wang, R.; Hu, C.; Yan, F.; Chadli, M. Composite Nonlinear Feedback Control for Path Following of Four-Wheel Independently Actuated Autonomous Ground Vehicles. *IEEE Trans. Intell. Transp. Syst.* **2016**, *17*, 2063–2074. [CrossRef]

23. Wang, R.; Jing, H.; Chen, N.; Zhang, H. Robust lateral-plane motion control of four-wheel independently actuated electric vehicles. In Proceedings of the 11th World Congress on Intelligent Control and Automation, Shenyang, China, 29 June–4 July 2014; pp. 1974–1979.

24. Zhang, H.; Zhang, X.; Wang, J. Robust gain-scheduling energy-to-peak control of vehicle lateral dynamics stabilisation. *Veh. Syst. Dyn.* **2014**, *52*, 309–340. [CrossRef]

25. Wang, R.; Jing, H.; Wang, J.; Chadli, M.; Chen, N. Robust output-feedback based vehicle lateral motion control considering network-induced delay and tire force saturation. *Neurocomputing* **2016**, *214*, 409–419. [CrossRef]

26. Du, H.; Zhang, T.; Dong, G. Stabilizing Vehicle Lateral Dynamics with Considerations of Parameter Uncertainties and Control Saturation Through Robust Yaw Control. *IEEE Trans. Veh. Technol.* **2010**, *59*, 2593–2597. [CrossRef]

27. Cao, Y.-Y.; Lin, Z. Robust stability analysis and fuzzy-scheduling control for nonlinear systems subject to actuator saturation. *IEEE Trans. Fuzzy Syst.* **2003**, *11*, 57–67. [CrossRef]

28. Nguyen, A.-T.; Sentouh, C.; Popieul, J.-C. Driver-Automation Cooperative Approach for Shared Steering Control under Multiple System Constraints: Design and Experiments. *IEEE Trans. Ind. Electron.* **2017**, *64*, 3819–3830. [CrossRef]

29. Wu, F.; Lu, B. Anti-windup control design for exponentially unstable LTI systems with actuator saturation. *Syst. Control Lett.* **2004**, *52*, 305–322. [CrossRef]

30. Falcone, P.; Borrelli, F.; Asgari, J.; Tseng, H.E.; Hrovat, D. Predictive Active Steering Control for Autonomous Vehicle Systems. *IEEE Trans. Control Syst. Technol.* **2007**, *15*, 566–580. [CrossRef]

31. Yu, S.; Li, X.; Chen, H.; Allgöwer, F. Nonlinear model predictive control for path following problems. *Int. J. Robust Nonlinear Control* **2014**, *25*, 1168–1182. [CrossRef]

32. Da Silva, J.; Tarbouriech, S. Antiwindup design with guaranteed regions of stability: An LMI-based approach. *IEEE Trans. Autom. Control* **2005**, *50*, 106–111. [CrossRef]

33. Wu, F.; Soto, M. Extended anti-windup control schemes for LTI and LFT systems with actuator saturations. *Int. J. Robust Nonlinear Control* **2004**, *14*, 1255–1281. [CrossRef]

34. Tiwari, P.Y.; Mulder, E.F.; Kothare, M.V. Multivariable Anti-Windup Controller Synthesis incorporating Multiple Convex Constraints. In Proceedings of the 2007 American Control Conference, New York, NY, USA, 11–13 July 2007; pp. 5212–5217.

35. Tyan, F.; Bernstein, D.S. Anti-windup compensator synthesis for systems with saturation actuators. *Int. J. Robust Nonlinear Control* **1995**, *5*, 521–537. [CrossRef]

36. Tarbouriech, S.; García, G.; Da Silva, J.M.G.; Queinnec, I. *Stability and Stabilization of Linear Systems with Saturating Actuators*; Springer Science and Business Media: Berlin, Germany, 2011.

37. Tarbouriech, S.; Turner, M. Anti-windup design: An overview of some recent advances and open problems. *IET Control Theory Appl.* **2009**, *3*, 1–19. [CrossRef]

38. Wang, Q.; Zhou, B.; Wen, C.; Duan, G.-R. Output feedback gain scheduled control of actuator saturated linear systems with applications to the spacecraft rendezvous. *J. Frankl. Inst.* **2014**, *351*, 5015–5033. [CrossRef]

39. Ban, X.; Fen, W. Gain scheduling output feedback controller design for saturated linear plants. In Proceedings of the 31st Chinese Control Conference, Hefei, China, 25–27 July 2012.

40. Rajamani, R. *Vehicle Dynamics and Control*; Springer Science & Business Media: Berlin, Germany, 2011.

41. Chai, Y.W.; Abe, Y.; Kano, Y.; Abe, M. A study on adaptation of SBW parameters to individual driver's steer characteristics for improved driver–vehicle system performance. *Veh. Syst. Dyn.* **2006**, *44*, 874–882. [CrossRef]

42. Plochl, M.; Edelmann, J. Driver models in automobile dynamics application. *Veh. Syst. Dyn.* **2007**, *45*, 699–741. [CrossRef]

43. Wang, R.; Jing, H.; Hu, C.; Yan, F.; Chen, N. Robust $H\infty$ Path Following Control for Autonomous Ground Vehicles With Delay and Data Dropout. *IEEE Trans. Intell. Transp. Syst.* **2016**, *17*, 2042–2050. [CrossRef]